in other tissues, too. For example, in calcitonin-secreting cells from human medullary thyroid carcinoma, increased plasma Ca^{2+} initially depolarizes cells by reducing K^+ or Cl^- conductance. Secondarily, Ca^{2+} influx through voltage-gated Ca^{2+} channels elicits hormone secretion (*19*). Calcium sensitivity in taste cells is similar to glucose sensitivity in pancreatic β cells: the initial depolarization produced by glucose is also caused by a reduction of K^+ conductance (*20*).

In man, Ca^{2+} salts generally produce a salty-bitter taste (*6*). Other taste qualities, including sour and sweet, may also be mediated in part by a modulation of K^+ conductance in taste cells (*16, 17, 21*). However, it is unlikely that a single universal mechanism fully explains chemosensory transduction of such diverse taste qualities, and the mechanism whereby sour, bitter, and sweet sensations are distinguished remains a paradox. Presumably, other changes in addition to alterations in K^+ conductance are involved in generating receptor potentials in different classes of receptor cells. For example, denatonium, an intensely bitter compound in man, blocks K^+ conductance and releases Ca^{2+} from intracellular stores in a subset of cells in taste buds (*22*). Nonetheless, the fact that taste cells have a highly voltage-dependent K^+ conductance that can be modulated by a variety of chemical stimuli imparts a precise voltage sensitivity to taste responses. Small (<10 mV) changes in the resting potential can have a profound effect on the amplitude of receptor potentials by virtue of the voltage sensitivity of the resting K^+ conductance. This property could be an important link between taste sensitivity and metabolic processes that affect resting membrane potential, for example, activity of electrogenic ion transporters such as Na^+,K^+ adenosine triphosphatase, Ca^{2+} exchanger.

REFERENCES AND NOTES

1. S. D. Roper, *Annu. Rev. Neurosci.* **12**, 329 (1989).
2. P. Avenet and B. Lindemann, *J. Membr. Biol.* **112**, 1 (1989).
3. S. S. Schiffman, *Chem. Sens.* **15**, 129 (1990).
4. D. Junge and M. S. Brodwick, *Comp. Biochem. Physiol.* **35**, 623 (1970).
5. T. Sato, *Prog. Neurobiol. (N.Y.)* **14**, 25 (1980).
6. R. W. Moncrieff, *The Chemical Senses* (CRC, Cleveland, 1967).

6a. Y. Kitada, *Jpn. J. Physiol.* **28**, 413 (1978).

7. S. C. Kinnamon and S. D. Roper, *J. Gen. Physiol.* **91**, 351 (1988).
8. S. D. Roper and D. W. McBride, Jr., *J. Membr. Biol.* **109**, 29 (1989).
9. P. Avenet and B. Lindemann, *ibid.* **95**, 265 (1987).
10. M. McPheeters and S. Roper, *Chem. Sens.* **10**, 341 (1985).
11. Mud puppies were rapidly decapitated and the tongues removed. The lingual epithelium was gently freed by blunt dissection and affixed with cyanoacrylic glue to a section of carrot. Thin slices (200 μm) were cut with a tissue chopper while the tissue was kept moist with chilled APS. Slices were scanned, and those containing taste buds were selected for electrophysiological experiments.
12. APS: 112 mM NaCl, 2 mM KCl, 8 mM $CaCl_2$, 5 mM Hepes, buffered to pH 7.2 with NaOH. Elevated Ca^{2+} concentrations facilitated stable intracellular impalements.
13. S. C. Kinnamon and S. D. Roper, *J. Physiol. (London)* **383**, 601 (1987).
14. We prepared chemical stimuli by dissolving $CaCl_2$ (200 mM), $BaCl_2$ (200 mM), and KCl (100 mM) in APS. Ba^{2+} was tested because it mimics the action of Ca^{2+}. KCl is a known stimulus for taste cells and was used both to establish the position of the multibarreled micropipette and to monitor the apical, resting K^+ conductance (*8, 16*). Stimulating solutions were applied focally to the apical membrane of taste cells from triple-barreled micropipettes (tip diameter, 10 to 15 μm). The perfusion system (3 to 5 ml/min) directed APS over the taste bud and thus rapidly removed chemical stimuli after their application to the taste pore (monitored with Fast Green dye). Chemical stimuli were prevented from reaching the basolateral surfaces of the taste cells. The concentration at the apical membrane of the taste cells was lower than the concentration applied as a result of dissipation in the bath. On the basis of the Nernst equation [assuming the intracellular K^+ concentration to be 80 mM (*16*)] and the peak amplitude of KCl responses, we estimated a peak KCl concentration at the taste cell membrane of 20 to 30 mM, corresponding to a three- to fivefold dilution from the concentration in the stimulating pipette. By using this dilution factor for $CaCl_2$ and $BaCl_2$, we calculated their concentrations at the apical membrane to be 40 to 60 mM. These concentrations are higher than those used in taste experiments in the intact animal (*3*). This difference is because tissue slices, especially the apical ends of taste cells, are bathed in a solution of saline that causes adaptation. This raises the threshold of excitation to Ca^{2+} salts (*3, 6a*).

14a. S. C. Kinnamon, T. A. Cummings, S. D. Roper, K. G. Beam, *Ann. N.Y. Acad. Sci.* **560**, 112 (1989).

15. C. M. Armstrong and D. R. Matteson, *J. Gen. Physiol.* **87**, 817 (1986); B. Rudy, *Neuroscience* **25**, 729 (1988); J. B. van de Mortel, A. P. Theuvenet, G. W. Borst-Pauwels, *Biochim. Biophys. Acta* **1026**, 220 (1990).
16. S. C. Kinnamon and S. D. Roper, *Chem. Sens.* **13**, 115 (1988).
17. S. C. Kinnamon, V. E. Dionne, K. G. Beam, *Proc. Natl. Acad. Sci. U.S.A.* **85**, 7023 (1988).
18. N. Akaike, A. Noma, M. Sato, *J. Physiol. (London)* **254**, 87 (1976); K. Kurihara, in *Biosignal Transduction Mechanism*, M. Kasai, T. Yoshioka, H. Suzuki, Eds. (Japan Scientific Society Press, Tokyo/Springer-Verlag, Berlin, 1989), pp. 181–205.
19. O. Sand, L. Jonsson, M. Nielsen, R. Holm, K. M. Gautvik, *Acta Physiol. Scand.* **126**, 173 (1986).
20. F. M. Ashcroft, D. E. Harrison, S. J. H. Ashcroft, *Nature* **312**, 446 (1984).
21. K. Tonosaki and M. Funakoshi, *ibid.* **331**, 354 (1988).
22. M. H. Akabas, J. Dodd, Q. Al-Awqati, *Science* **242**, 1047 (1988); A. I. Spielman *et al.*, *Brain Res.* **503**, 326 (1989).

23. We thank P. Avenet, R. Delay, D. Ewald, and S. Kinnamon for critical review of the manuscript. Supported in part by NIH grants 2 PO1 NS 20486, 5 RO1 AG06557, and 2 RO1 NS24107.

9 November 1990; accepted 1 February 1991

Low-Resolution Real-Space Envelopes: An Approach to the Ab Initio Macromolecular Phase Problem

S. SUBBIAH

An ab initio approach to the phase problem in macromolecular x-ray crystallography is described. A random gas of hard-sphere point scatterers is allowed to condense under the constraint of the solvent fraction and the restraint of the observed Fourier amplitude data. Two applications to real macromolecular examples are discussed. This method produces an approximate outline of the bulk solvent regions and thus yields a low-resolution picture of the unit cell that can be extended to higher resolutions in special cases, such as through the use of molecular replacement or of noncrystallographic symmetry-based phase extension.

THE PHASE PROBLEM IS A SEVERE rate-limiting step in macromolecular x-ray structure determination (*1*). Simply stated, the diffraction pattern of a crystal gives only the amplitudes of the Fourier transform of the crystal contents; the phase angle is lost. In principle, provided enough unique diffraction amplitudes are known, the many constraints imposed by a knowledge of general molecular structure make the inversion of the known Fourier amplitudes, in the absence of any phase information, into real-space electron density an overdetermined problem (*2*). However, theoretical methods, such as the direct method or the Patterson method (*3*), that exploit this overdeterminacy are presently only available for small molecules (typically fewer than 100 nonhydrogen atoms).

Much work has gone into the extension of direct methods to macromolecules (*1*), the exploration of the maximum entropy (ME) method for both the small molecule and macromolecule case (*4*), and the use of simulated annealing in both reciprocal and Patterson space for small molecule test cases (*5*).

Virtually all macromolecular x-ray phases have been obtained by experimental means, such as multiple isomorphous replacement (MIR), MIR supplemented by anomalous scattering data, single isomorphous replacement (SIR) supplemented by anomalous scattering data, and recently the multiple wavelength method when suitable anoma-

Beckman Laboratories for Structural Biology, Department of Cell Biology, Stanford University School of Medicine, Stanford, CA 94305.

lous scatterers are present in the unit cell (*6*). Recent work has described the direct measurement of centric phases (*7*).

In special situations, theoretical methods can be used to solve macromolecular structures. Despite frequent failure in practice, when a sufficiently similar homologue model is available, the phase problem can often be circumvented by the technique of molecular replacement (MR) (*8*). When threefold or greater noncrystallographic symmetry is present and a molecular envelope is available from electron microscopy or from SIR data, appropriate symmetry averaging can often be robust enough to result in successful phase extension to higher resolution, as in virus crystallography (*9–11*).

A simple technique has been developed to obtain a very low resolution picture (about 10 to 15 Å) of the unit cell contents from a completely random start in which only one piece of information is assumed, namely, a rough estimate of the solvent fraction or equivalently a rough estimate of the number of scattering atoms in the asymmetric unit. For instance, if the true solvent fraction is 40%, the method I discuss should work if the estimate supplied is anywhere between 20 and 60%. Similarly, the estimate of the number of scattering atoms present can be in error by 20% or so. It is given that the space group and unit cell dimensions are known and that a Fourier amplitude data set, with a $R_{sym} \sim 0.1$ and the usual levels of completeness, is available to at least 7 or 8 Å resolution.

Regardless of the size of the macromolecule, the method should readily produce a low-resolution envelope of the macromolecule. In practice, surface features and some internal features that are typical of ~10 Å resolution can be observed. The envelopes are of sufficient merit to easily identify the presence of and reliably fit any available homologue model. Local rigid-body refinement can then lead to a proper phase start at higher resolution (*12, 13*). These real-space envelopes are of sufficient quality to replace the less reliable traditional molecular replacement methods that operate in reciprocal space. They are also of sufficient quality to locate and identify large domains within the macromolecule, thus conceivably allowing a bootstrap from a partial homologue model to higher resolution (traditional molecular replacement with partial models often fails). In cases where noncrystallographic symmetry is present, the results obtained are sufficient to readily locate the individual copies of the macromolecule in the asymmetric unit.

The general strategy is that a random gas of similar hard-sphere point scatterers is allowed to condense under the constraint of (i) the packing fraction and the restraint of (ii) the observed Fourier amplitude data. The first three steps establish the packing constraint, the next two establish the Fourier restraint, and the last step documents the scheduling of the condensing procedure. The target image sought is the negative image and not the positive one; I discuss below why the point scatterers are expected to move into the solvent void.

1) An estimate of the number of Cα atoms, N_{ca}, present in the asymmetric unit gives a rough idea of the number of point scatterers that can simultaneously be spaced at 3 to 4 Å intervals along the protein backbone and so capture the spirit of the fold.

2) The number and physical characteristics of such hard-sphere point scatterers that can optimally satisfy the expected packing fraction P are chosen. Such optimal packing must allow for the gas of scatterers to have sufficient mobility at all times during the condensation process. The following discussion first estimates the number of hard-sphere point scatterers of radius 1.5 Å that are required to optimally and randomly pack the volume occupied by the bulk solvent in typical crystals, N_{op}. Allowance must be then made for sufficient mobility within such a gas of scatterers. Typical protein crystals of unit cell volume V have a solvent content of $\sim 0.4\ V$ (or $P = 0.6$). The theoretical value for the maximal packing fraction of random hard spheres is ~0.6 (*14*). These last two observations together imply that the most optimal packing of these hard spheres in the bulk solvent void external to the low-resolution macromolecular envelope requires $N_{op} \approx (0.24\ V)/[(4/3)\pi(1.5)^3]$ of them. The requirement that the gas be sufficiently fluid at all times demands that this number be significantly smaller. Moreover, any lower bound on the step size of the smallest moves that the scatterers are allowed to make further restricts this optimal number of mobile scatterers. Even more severe limitations on mobility are imposed by the Fourier restraints. Thus one expects this to decrease the previous estimate for N_{op}. Empirically, the optimal number of sufficiently mobile scatterers N_{hs} is between 0.04 and 0.08 times $V/[(4/3)\pi(1.5)^3]$. Incidentally, for typical values of P (0.5 to 0.6), N_{ca} is ~1.5 times the values considered here for N_{hs}; thus a general strategy that works well in practice is to use $0.67\ N_{ca}$ random scatterers.

3) The asymmetric unit is loosely and randomly filled with $N_{hs} = 0.67\ N_{ca}$ hard-sphere point scatterers of radius 1.5 Å. Each hard sphere is treated as a single point scatterer of scattering factor unity. Thus a simple intersphere collision distance of 3 Å is implemented, as opposed to a treatment that involves uniform mass distributed over a sphere of radius 1.5 Å. Hence this fairly mobile gas of simple point scatterers cannot provide a phase description of matter to better than 3 Å resolution.

4) The available experimental Fourier amplitude data $|F_o|$ should typically be mostly complete to at least 7 or 8 Å. The data are then converted to the standard normalized $|E_o|$ values that are conventionally used in direct methods (*2, 15*). This correction has little effect at resolutions below 4 or 5 Å.

5) Normalized Fourier amplitudes $|E_c|$ are then calculated by simple trigonometric summation over the random starting configuration of N_{hs} hard spheres. The standard Pearson correlation coefficient, $r = [\Sigma(|E_o| - \langle|E_o|\rangle)(|E_c| - \langle|E_c|\rangle)]/[\Sigma(|E_o| - |E_o|)^2\Sigma(|E_c| - \langle|E_c|\rangle)^2]^{1/2}$, is computed for this configuration. To first order, this formula of assessing the goodness of fit between model and data avoids the problem of correctly scaling the calculated data set with the observed data set. The choice of resolution K to which the two data sets are compared is primarily dependent on two conditions. First, the resolution cannot exceed the intercollision distance of 3 Å. Second, there should be sufficient overdeterminacy: typically a few hundred reflections suffice and the use of more reflections makes little difference. For instance, when a large unit cell is being considered, data to 7 or even 10 Å should offer ample overdeterminacy. For smaller unit cells, sufficient overdeterminacy can be attained at 4 or 5 Å resolution.

6) The general strategy is to randomly select one of the N_{hs} hard spheres and move it a distance x in one of the six directions defined by the unit cell edges. Moves that would cause hard spheres to interpenetrate are rejected. The value of r is recalculated. If r is favorable (maximized), the move is accepted; otherwise it is rejected. The procedure is repeated for another hard sphere. Each such repetition is defined to be a microcycle. The number of microcycles that are attempted I_t, the number of microcycles that result in accepts I_a, and the number of microcycles that result in rejects I_r are monitored (by necessity, $I_t = I_a + I_r$). When 10 accepts occur before a total of 100 attempts has been considered, the collection of attempts is collectively defined as a condensing macrocycle. If the target quota of $I_a = 10$ has not been attained within $I_t = 100$ attempts, the set of 100 microcyles is labeled a condensed macrocycle. Many, but no more than 200, consecutive macrocycles at a given value of move step size x together constitute a supercycle. A supercycle terminates prematurely if 40 condensed macrocycles occur consecutively; x is then decreased before the

next supercycle is performed. Thus, consecutive supercycles are carried out with the value of x typically decreasing in integral angstrom units from x_i to x_f. Ordinarily, the initial move step size x_i is chosen to be anywhere between one half and one quarter of the average dimensions of the asymmetric unit. The final move step size x_f need not be much smaller than the resolution k of the supplied data. This particular scheduling of move step sizes is designed to perform coarse and large moves that can readily span the full asymmetric unit first. Subsequent moves sample the experimental Fourier data more finely. As to be expected on the basis of Fourier sampling considerations, move step sizes finer than about one third of the resolution K contribute little to the final outcome. This entire procedure—from the first supercycle to the last one—is called the condensing protocol. When the last supercycle is terminated, the value of r will typically be about 0.6 to 0.8. This value is to be compared with the typical values of $r \sim 0$ for random starting configurations (r can range from -1 to 1). At this point, direct visualization of the spatial distribution of the condensed scatterers within the asymmetric unit with molecular graphics software (*16*) can outline the molecular envelope and can also show some low-resolution features, such as interdomain clefts and other prominent surface indentations (*17*).

The first test case was the protein structure of the elastase molecule from *Pseudomonas aeruginosa*, which was originally solved in the absence of ligand in space group $P2_1$ by Thayer, Flaherty, and McKay (*18*). More recently, this 298-residue molecule has been crystallized in the presence of an inhibitor, phosphoramidon, in space group $P2_12_12_1$, with one molecule per asymmetric unit (unit cell dimensions are $a = 124.4$ Å, $b = 51.5$ Å, and $c = 44.5$ Å), and its structure has been solved (*19*). Structure factors from the orthorhombic space group were used in this test. The packing fraction P is ~0.6. Thus, a unit cell has four symmetry-related solvent voids that together account for 40% of the unit cell volume; 70% of the data to 2.0 Å was collected with an R_{sym} of 0.035, and 86% of the data to 7 Å was collected with an R_{sym} of 0.021. The low-resolution cutoff was 40 Å. The current refined R factor to 2 Å is 0.178. This experimental native data set was used to determine the low-resolution molecular envelope of elastase within its $P2_12_12_1$ unit cell. The parameters used were $N_{ca} = 298$, $N_{hs} = 199$, $N_{ref} = 470$ (number of unique reflections used), $K = 7$ Å, $x_i = 12$ Å, and $x_f = 8$ Å. The initial r value was -0.06. After about 40 min of cpu time, the condensing procedure resulted in an r value of 0.85. The raw primary data—the contents of the unit cell before and after this procedure—are shown in Fig. 1.

The condensed point scatterers preferentially fill the solvent void. These point scatterers outline the molecular envelope; Fig. 1C shows evidence for surface features on the order of 10 Å. In order to assess the accuracy more quantitatively, a 15 Å envelope of the elastase model was made on a 2 Å grid. The envelope was chosen such that 50% of the grid points corresponding to the highest electron density fell within it. The accuracy of the low-resolution prediction was crudely assessed in terms of the spatial distribution ratio j, which is defined as the number of point scatterers that fall outside this envelope divided by the number that lie within. This ratio would be ~1 for an ideal random distribution of the point scatterers. As condensation proceeds and point scatterers move out of the envelope into the void, this ratio should increase. The values of j and r were monitored over every macrocycle; Fig. 2, A and B, shows that j increases from 1.11 to 1.93 while r increases from -0.06 to 0.85. Although j approximately discrimi-

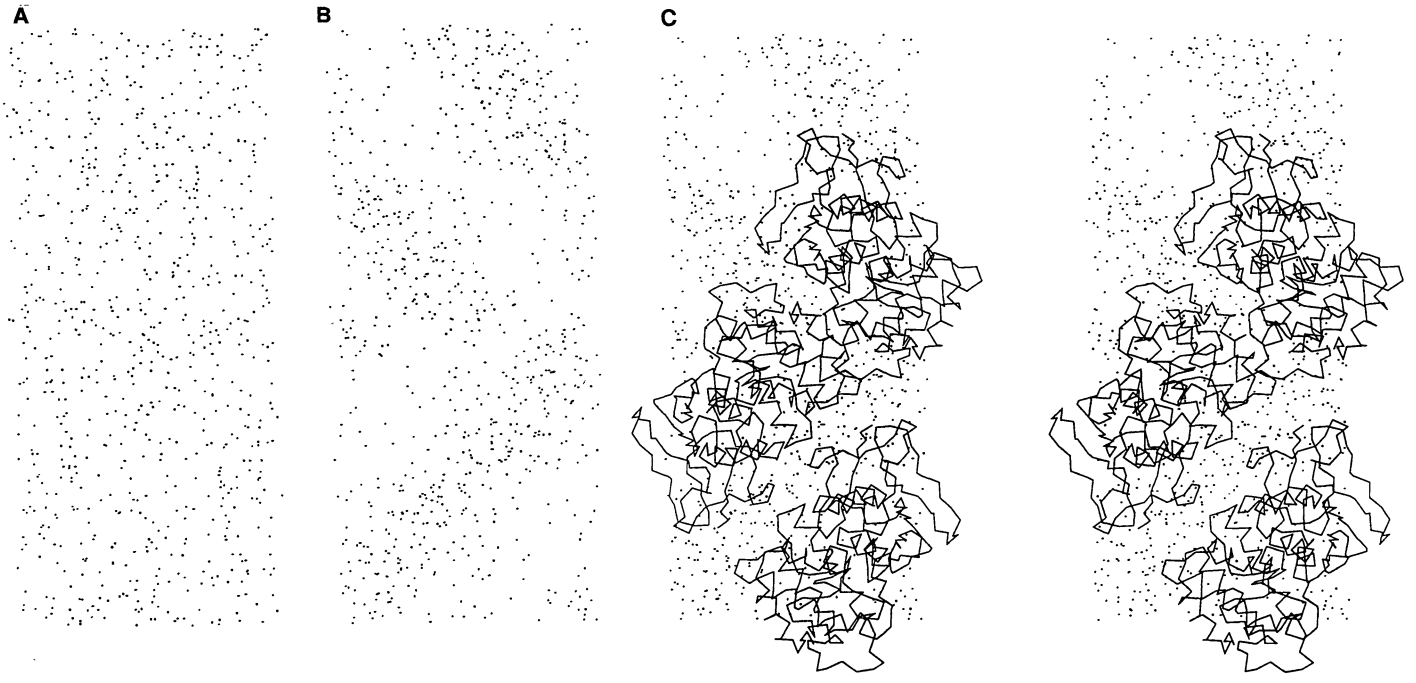

Fig. 1. The boxed contents of the full $P2_12_12_1$ unit cell of the elastase crystal. (**A**) All $N_{hs} = 199$ randomly positioned point scatterers (and their three symmetry-related sets) at the beginning of the protocol. (**B**) The same point scatterers at the end of the condensing protocol. The symmetry-related regions devoid of point scatterers are readily apparent even without the benefit of stereo. (**C**) This panel shows three symmetry-related copies of the Cα trace of the elastase model superimposed onto the figure in (B). The models are placed exactly as they occur in the unit cell of the crystals. For clarity the fourth symmetry-related model has been left out. Clearly, there is a "hole" ready to receive this fourth model at the top left of (C). As portions of these models extend outside of the cuboid unit cell, there should be compensating small portions of other molecules that extend into the cuboid (left out for clarity). Particularly in (C), one can see that all of the point scatterers that would lie within a low-resolution molecular envelope tend to be near the periphery of such an envelope. The elastase molecule has two domains that are separated by a fairly deep cleft that is on the order of 10 Å across. In the view presented, the cleft lies at the very bottom right-hand corner of the cuboid. In stereo it lies closer toward the top of the page. Both in (B) and in (C), the 12 or so point scatterers that extend into this cleft can be easily seen.

nates between solvent and macromolecule, it does not capture the actual local spatial distribution of these point scatterers within either the solvent void or, more importantly, within the macromolecular envelope. In particular, in Fig. 1C, a stereo inspection of the condensed point scatterers shows that those that lie within the macromolecular envelope tend to be preferentially distributed toward the edges of the macromolecule rather than cluster about the molecular centroid. Similar results have been obtained both from different random starting configurations and by using different, but appropriate, resolution ranges. The coarse molecular envelopes obtained in this manner were sufficiently detailed to place the Cα model within a few angstroms of its true center of mass. A limited translational and rotational rigid-body R factor search with the use of standard programs could identify the exact location of the molecule within the unit cell (*13*). Likewise, in all other examples attempted it has been always possible to similarly refine the fitted homologue model to its true position. Therefore there has been no need to average over the results of several condensing cycles to improve the image quality. When such simple averaging was attempted, the quality of the results were not significantly improved.

The second test case was that of the DNA-binding domain of the repressor protein in the 434 phage, R1t69 (*20*). The 63-residue domain crystallized in $P2_12_12_1$, with one molecule per asymmetric unit (a = 32.8 Å, b = 37.5 Å, and c = 44.6 Å; $P \sim 0.6$). The unit cell has four symmetry-related solvent voids that together account for 40% of the unit cell volume. The crystals diffracted to 1.5 Å and in the original structure determination 96% of the data to 1.9 Å were collected with an R_{sym} of 0.054. The R_{sym} to 5 Å was 0.031. When older refinement methods that were not based on molecular dynamics were used, a final refined R factor of 0.19 was attained to 1.9 Å resolution. This experimental native data set was used with the method described above to determine the low-resolution molecular envelope of R1t69 within its $P2_12_12_1$ unit cell. The parameters used were N_{ca} = 63, N_{hs} = 43, N_{ref} = 291, K = 5 Å, x_i = 8 Å, and x_f = 3 Å. The requirement of sufficient overdeterminacy in the context of the smallness of this unit cell requires that data to a higher resolution than in the first example be used. Also, since the point scatterers are not as numerous as in the previous example, and since the unit cell is smaller, all allowable moves can be sampled with fewer macrocycles. Hence the minimium number of macrocycles per supercycle has been decreased from 40 to a more computer efficient 20.

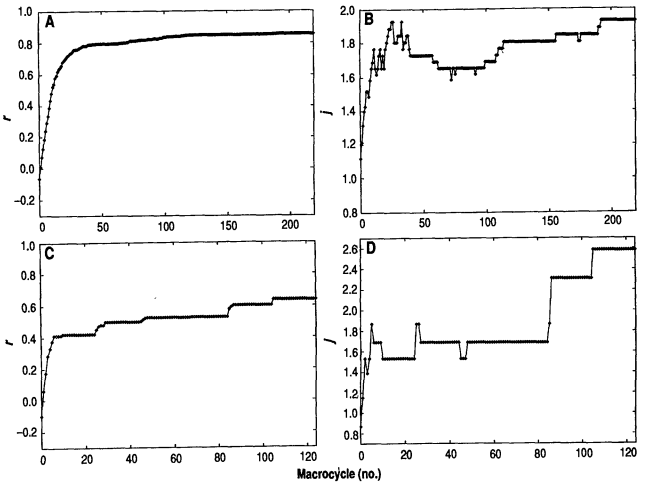

Fig. 2. The values r and j of the condensing point scatterers for elastase (**A** and **B**) and R1t69 (**C** and **D**). For elastase, the x-axis charts the 219 macrocycles that occured in that experiment. The initial step size of x_i = 12 Å was used for the first 59 macrocycles that constituted the first supercycle. The remaining four supercycles, each of 40 macrocycles, were conducted at integrally decreasing step sizes to a final step size of x_f = 8 Å. A few point scatterers may rearrange themselves during the many microcycles that occur within a given macrocycle. These rearrangements could be such that r increases without any point scatterer ever crossing the envelope boundary during a given macrocycle. Further, a single point scatterer, among the many present, may move into the envelope while causing a modest increase in r. There is no contradiction in this observation since it applies to the motion of one or a few scatterers against a backdrop of the many point scatterers that describe the macrolevel spatial distribution. More specifically, the rather large step sizes used—very substantial fractions of the asymmetric unit dimensions—limit the available locations to which a given scatterer may randomly move. Therefore a depletion of a particularly overfilled and densely populated region outside the envelope by one point scatterer may enable a modest increase in r—even if this point scatterer is forced to move to a location that is within the molecular envelope. This scenario would appear particularly attractive when the destination is in the internal periphery of the molecular envelope as opposed to the more central core of the envelope. In fact, this would explain the general distribution of the point scatterers that lie within the molecular envelope in Fig. 1C. For R1t69, the x-axis charts the 124 macrocycles that are spread over six supercycles. The first supercycle, in which a step size x_i = 8 Å was used, contains 24 macrocycles. The other five supercycles at integrally decreasing step sizes each contain 20 macrocycles. In the last supercycle a step size of x_f = 3 Å was used.

The initial r value was −0.1. The initial value of j was 0.87. This value is <1 and illustrates that the initial starting configuration can even be somewhat unfavorable. After about 10 min of cpu time, the condensing procedure resulted in an r value of 0.65 and a j value of 2.6. As before, Fig. 3 shows the primary data and Fig. 2, C and D, details the progress of the condensation process. The index of spatial distribution j was calculated as described above but with a 6 Å envelope of the R1t69 model made on a 2 Å grid. A 15 Å envelope as in the elastase case would not have been possible as the unit cell dimensions limit the number of available reflections at very low resolution.

Similar results have been obtained with other proteins in other space groups as well. In principle, the method is just as applicable to DNA structures. In fact, the method could in principle be a general one for any problem that requires phaseless Fourier inversion at low resolution.

The reasons why the target image for the condensation protocol is the negative image (the solvent void) and not the positive one (the macromolecule itself) are as follows. When a Fourier amplitude is squared, its sign is lost. Thus a correlation coefficient based on the relative differences in the magnitude of |**F**|'s (or equivalently |**E**|'s) cannot discriminate between a featureless negative image and a featureless positive image. As the protocol condenses, the refined gas of homogenous and featureless scatterers may equally well fill a featureless macromolecular volume or a featureless solvent void. However, the approximation that both the solvent and the macromolecule are featureless is not valid beyond some extremely low resolution. At most resolutions, even the low ones considered here, the macromolecule has much internal variation in local density. In contrast, the solvent void is essentially featureless. Thus, the gas of scatterers considered here can inherently match the negative image more readily. However, very infrequently, and particularly under a "poor" choice of parameters, a positive image can be obtained. The envelopes so obtained appear to be of inferior quality when compared to those obtained through the much more stable negative image. The sign of a given resultant image can be readily assessed by a suitable density-based refinement of the resultant image as compared to its inverse. More explicitly, the condensed scatterers can be allowed to have variable ability to scatter x-rays. Particularly at higher resolutions, this should allow discrimination between the solvent and the macromolecule.

The method appears to be powerful for two important reasons. The concept of a freely mobile gas of independent scatterers

affords many different ways in which the same global minimum can be obtained as the gas condenses subject to the native Fourier amplitude data restraints. The appropriate choice of the hard-sphere radius imposes a critical packing constraint and ensures that the available Fourier amplitude data is not oversampled, which would lead to the nearest uninteresting local minimum. The second critical point is the choice of resolution K and its appropriateness with regard to both the numbers of scatterers and their hard-sphere radii. For example, if the initial move step size x_i is less than K, the condensation procedure is unstable and the many allowable small local moves lead the protocol to the nearest local minimum. (When x_f is much smaller than K, nothing untoward, outside of increased computational effort, happens as long as the companion x_i has been chosen to be suitably larger than K.) In general, the topological features of the solution space seen by the algorithm can be regulated by a suitable choice of these three parameters—K, N_{hs}, and the hard-sphere radius. Enhancing and regulating these features can present a suitably strong gradient that allows convergence to the global minimum or its near vicinity. In other words, under the correct set of conditions, many local minima that lie en route between the random start point and the global minimum can be suppressed. This gradient, in conjunction with the many different paths available to the global minimum and the overdeterminacy inherent in the supplied Fourier amplitude data, is sufficient to allow direct minimization from any random start configuration to the low-resolution global minimum or a local minimum that is sufficiently near that global minimum.

The low-resolution technique appears to be good enough to ultimately result in high-resolution structure determination in the following special cases: (i) traditional molecular replacement with full or partial models; (ii) phase extension based on three- or more fold noncrystallographic symmetry (*10*); (iii) available high-resolution SIR data; (iv) two-dimensional and three-dimensional tilt electron microscopy, where Fourier data are typically of higher resolution than the available direct phases (*21*); and (v) verification of the goodness of candidate heavy-atom data sets. Beyond these possible applications the method could be of potential use in complementing present methods that seek to solve the ab initio phase problem at higher resolutions. It could also provide a low-resolution phaseless Fourier inversion scheme for Fourier problems other than the crystallographic one. The method is not in any fundamental way specific to the low-resolution range considered in the context of this report; the same or a related strategy could be directly applicable to higher resolution.

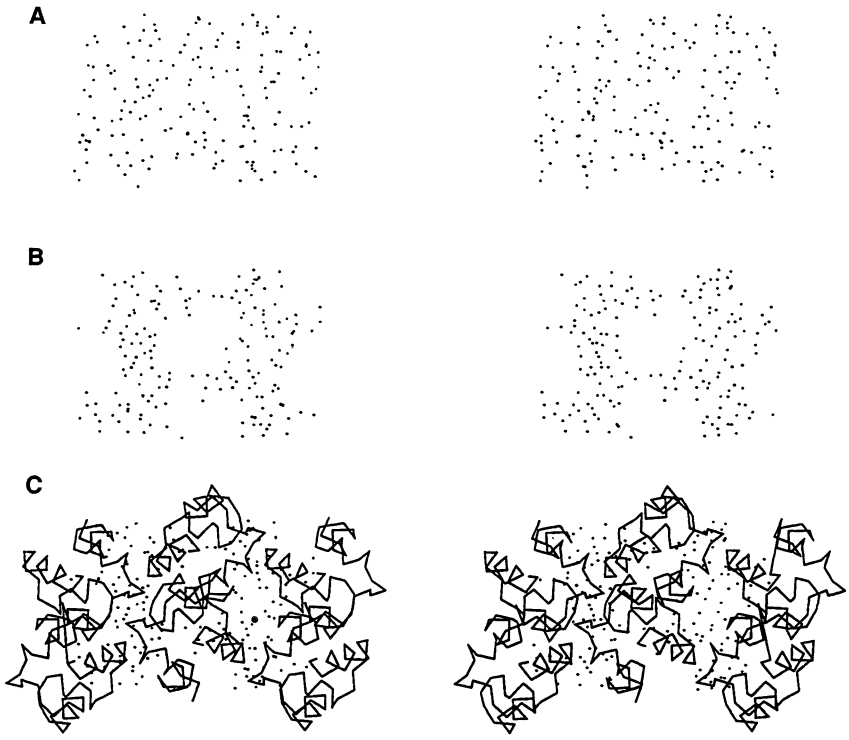

Fig. 3. The boxed contents of the full $P2_12_12_1$ unit cell of the 434 R1t69 crystal. (**A**) All N_{hs} = 43 randomly positioned point scatterers (and their three symmetry-related sets) at the beginning of the protocol. (**B**) The same point scatterers are shown at the end of the condensing procedure. (**C**) For comparison six copies of the R1t69 Cα trace—placed in their proper orientations within the unit cell—are shown superimposed on (B). Some of these models extend out of the unit cell. For reasons of clarity, portions of two other copies of the R1t69 model which extend into the boxed unit cell have been omitted. One of these happens to fill the small region at the bottom center of (C) that is empty of point scatterers. In general, the point scatterers are more densely present in the solvent channel areas. The scatterers that would fall within the molecular envelope tend to lie near the envelope.

REFERENCES AND NOTES

1. J. Karle, *Acta Crystallogr.* **A45**, 765 (1989).
2. ———, *Science* **232**, 837 (1986).
3. ——— and H. Hauptman, *Acta Crystallogr.* **3**, 181 (1950); H. Hauptman, *Crystal Structure Analysis: The Role of Cosine Seminvariants* (Plenum, New York, 1972); A. L. Patterson, *Phys. Rev.* **46**, 372 (1934).
4. D. M. Collins, *Nature* **298**, 49 (1982); G. Bricogne, in *Computational Crystallography*, D. Sayre, Ed. (Oxford Univ. Press, New York, 1982), pp. 258–264; P. L. Britten and D. M. Collins, *Acta Crystallogr.* **A38**, 12 (1982); R. Narayan and R. Nityananda, *ibid.*, p. 122; S. W. Wilkins, J. M. Varghese, M. S. Lehmann, *ibid.* **A39**, 47 (1983); O. E. Piro, *ibid.* p. 61; J. Navaza, *ibid.* **A41**, 222 (1985); E. Prince, L. Sjolin, L. A. Svensson, *ibid.* **A44**, 218 (1988); G. Bricogne, *ibid.* **A40**, 410 (1984); A. Klug, *ibid.* **11**, 515 (1958).
5. N. Metropolis, A. Rosenbluth, M. Rosenbluth, A. Teller, E. Teller, *J. Chem. Phys.* **21**, 1087 (1953); S. Kirkpatrick, C. D. Gelatt, Jr., M. P. Vecchi, *Science* **220**, 671 (1983); S. V. Semenovskaya, K. A. Khachaturyan, A. G. Khachaturyan, *Acta Crystallogr.* **A41**, 268 (1985); S. Subbiah, unpublished results.
6. J. Karle, *Int. J. Quantum Chem. Symp.* **7**, 357 (1980); W. A. Hendrickson *et al.*, *Proc. Natl. Acad. Sci. U.S.A.* **86**, 2190 (1989).
7. W. N. Lipscomb, *Acta Crystallogr.* **2**, 193 (1949); B. Post, *ibid.* **A35**, 17 (1979); W. Shen and R. Collela, *Nature* **329**, 232 (1987).
8. M. G. Rossman and D. M. Blow, *Acta Crystallogr.* **15**, 24 (1962).
9. G. Bricogne, *ibid.* **23**, 832 (1976).
10. A. Podjarny, T. N. Bhat, M. Zwick, *Annu. Rev. Biophys. Biophys. Chem.* **16**, 351 (1987), and references therein.
11. E. Arnold and M. G. Rossman, *Proc. Natl. Acad. Sci. U.S.A.* **83**, 5489 (1986).
12. J. L. Sussman, S. R. Holbrook, G. R. Church, S. H. Kim, *Acta Crystallogr.* **A33**, 800 (1977).
13. A. T. Brünger, J. Kuriyan, M. Karplus, *Science* **235**, 458 (1987).
14. H. S. M. Coxeter, *Introduction to Geometry* (Wiley, Toronto, ed. 2, 1961), pp. 404–410.
15. A. J. C. Wilson, *Acta Crystallogr.* **2**, 318 (1949).
16. T. A. Jones, *J. Appl. Crystallogr.* **11**, 268 (1978).
17. The computing time needed is modest. The condensing protocol for most macromolecular problems of interest requires on the order of 1 hour of cpu (central processing unit) time or less on a VAX 8550). Many of the parameters discussed above that have not been singled out to be critical can be varied without drastically altering performance. For instance, the number of microcycles, macrocycles, and supercycles can be modified; however, at any time these cycles must be sufficient in number to sample all of the allowable moves well. Even the hard-sphere radius can be modified if the restraints imposed by the available resolution are not exceeded and the scheduling of step sizes is kept compatible. Although a Monte Carlo–type maximization [D. A. Keen and R. L. McGreevy, *Nature* **344**, 423 (1990)] is conducted here, the procedure is robust enough to work under a wide variety of standard multidimensional maximization schemes—conjugate gradient methods, downhill simplex method, direction-set methods, variable metric methods, and the simulated annealing method. The essence of the scheme is quite unrelated to the maximization method used but is rather rooted in the selection of the parameters that define the condensing gas of scatter-

ers. Although r is maximized, the scheme can also work when instead the standard properly scaled crystallographic R factor is minimized.
18. M. Thayer, K. M. Flaherty, D. McKay, *J. Mol. Biol.*, in press.
19. K. M. Flaherty *et al.*, unpublished results.
20. A. Mondragon, S. Subbiah, S. C. Almo, M. Drottar, S. C. Harrison, *J. Mol. Biol.* **205**, 189 (1989).
21. P. T. Unwin and R. Henderson, *ibid.* **94**, 425 (1975).
22. I am deeply indebted to A. Haykhov, M. Babyoneshev, P. Rosenthal, and T. B. Splott for their irrational faith, G. Petsko for arranging a home for this work, M. Levitt and everyone in his group—M. Steffey, M. Hirschberg, C. Lee, B. Park, D. Hinds, N. Kuhn and V. Daggett—for giving me that home and more (NIH grant GM-41455), D. McKay and in particular, K. Flaherty, for being exceptionally generous neighbors, R. Kornberg for invaluable help, and the Damon Runyon–Walter Winchell Postdoctoral Fund (DRG-1019) for my stay at Stanford.

3 August 1990; accepted 11 January 1991

Technical Comments

Treating Parkinson's Disease with Lesions of the Subthalamic Nucleus

We would like to caution against reviving ablation therapies for the treatment of Parkinson's disease, as was suggested by H. Bergman *et al.* (*1*). The authors report that unilateral lesioning of the subthalamic nucleus (STN) with ibotenic acid injection reduced all of the major motor disturbances in the contralateral limbs of two monkeys rendered parkinsonian by systemic treatment with 1-methyl-4-phenyl-1,2,3,6-tetrahydropyridine (MPTP). They postulate that the motor abnormalities seen in the MPTP model of Parkinson's disease were the result of excessive activity in the STN, which increased inhibitory output of the internal division of the globus pallidus (GPi). They suggest that surgical or pharmacological inactivation of the STN should be studied as a potential clinical therapy for this movement disorder.

Using the MPTP model in cynomologus monkeys (*Macaca fascicularis*) (*2*), we evaluated the role of polymer-encapsulated, dopamine-secreting cells in reversal of experimental parkinsonism (*3*). We evaluated tremor and rigidity with qualitative observations of behavior. We quantified akinesia for each upper limb by measuring the time required for a monkey to empty a tray of small wells loaded with food treats (*4*). Fifteen animals showed the typical parkinsonian akinesia contralateral to the carotid injection. Their ability to pick food from the tray was either completely or significantly impaired. One animal showed nearly complete unilateral loss of dopaminergic cells in the substantia nigra (SN). It did not show the typical parkinsonian symptoms, but demonstrated normal performance at the picking test even after two consecutive MPTP injections (0.6 and 0.3 mg/kg) 7 weeks apart. Ten weeks after the second injection this animal was killed . Tyrosine hydroxylase immunohistochemistry revealed severe lesions in the SN pars compacta comparable to that seen in our hemiparkinsonian animals (Figs. 1, A and B). Macroscopic observation and cresyl violet staining of slides revealed that a vascular lesion, possibly caused by an air embolism created during the carotid injection of MPTP, also destroyed the GPi (Fig. 1, C and D). In this monkey suppression of the inhibitory output of the GPi apparently prevented the development of typical parkinsonian symptoms, including akinesia.

Coagulative lesions of the GPi or of its thalamic projection targets have reduced tremor and rigidity in human Parkinson's patients without any effect on akinesia (*5*). The absence of parkinsonism in a primate with a combined lesion of both the SN and the GPi indicates that the pathophysiology of idiopathic Parkinson's disease may be more complex than that suggested by the MPTP model, or that the pallidectomies performed in humans were not sufficiently restricted to the GPi.

STN lesions could only modify the output of the GPi. Further animal studies should be conducted so that we understand the discrepancy between the results of lesioning the GPi in an MPTP model and the results of thalamotomies or pallidectomies that have been performed for the treatment of human idiopathic Parkinson's disease.

PATRICK AEBISCHER
MOSES GODDARD
Division of Biology and Medicine,
Brown University,
Providence, RI 02912

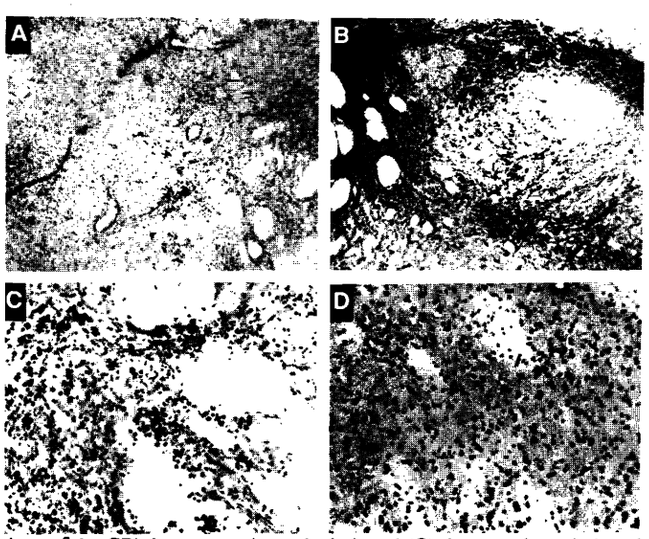

Fig. 1. Tyrosine hydroxylase (TH) immunostain (Incstar) demonstrate an absence of the dopaminergic pars compacta cells of the SN on the lesioned (**A**) and the unlesioned (**B**) sides. Free-floating sections were treated with a monoclonal antibody to TH (Incstar, Stillwater, Minnesota), followed by secondary rabbit antibodies to mouse, and a mouse peroxidase–antiperoxidase complex (Sternberger-Meyer, Jarrettsville, Maryland). The reaction is made visible by enzyme histochemical techniques and counterstaining with cresyl violet. Cresyl violet–stained sections of the GPi show necrosis on the lesioned (**C**), but not the unlesioned (**D**) side. Magnification, ×100.

REFERENCES

1. H. Bergman, T. Wichmann, M. R. DeLong, *Science* **249**, 1436 (1990).
2. K. S. Bankiewicz *et al.*, *Life Sci.* **39**, 7 (1986).
3. P. Aebischer *et al.*, *Soc. Neurosci. Abstr.* **16**, 963 (1990).
4. P. Aebischer and W. Schultz, *Neurosci. Lett.* **50**, 24 (1984).
5. R. Meyers, *N.Y. State J. Med.* **42**, 317 (1942); T. Hirai, M. Miyazaki, H. Nakajima, T. Shibazaki, C. Ohye, *Brain* **106**, 1001 (1983); L. V. Laitinen and M. I. Hariz, *Movement Disord.* **5** (suppl. 1), 82 (1990).

18 October 1990; accepted 8 March 1991

Response: Our paper (*1*) was intended to be a contribution to the understanding of the pathophysiology of parkinsonian motor signs. It was not meant to be a proposal for new surgical treatments for Parkinson's dis-